Reinterpretation of Single-Wall Carbon Nanotubes by Raman Spectroscopy

Yeseul Park,[†,§,#,∇] K. P. S. S. Hembram,[†,#] Ran Yoo,[§] Byungjin Jang,[§] Wooyoung Lee,[§] Sang-Gil Lee,[∥] Jin-Gyu Kim,[∥] Yong-Il Kim,[⊥] Dong Ju Moon,[‡] Jeon-Kook Lee,[†] and Jae-Kap Lee*,[†]

[†]Opto-Electronic Materials and Devices Research Center, Korea Institute of Science and Technology (KIST), Seoul 02792, Republic of Korea

[§]Department of Materials Science and Engineering, Yonsei University, 262 Seongsanno, Seoul 03722, Republic of Korea

[∥]Division of Electron Microscopic Research, Korea Basic Science Institute, Daejeon 34133, Republic of Korea

[⊥]Frontier in Extreme Physics, Korea Research Institute of Standards and Science, Daejeon 34113, Korea

[‡]Clean Energy Research Center, Korea Institute of Science and Technology (KIST), Seoul 02792, Republic of Korea

Ⓢ *Supporting Information*

ABSTRACT: Raman spectra of single-wall carbon nanotubes (SWNTs) exhibit a unique radial breathing mode (RBM) band ($\sim$100−300 cm^{-1}) and a G$^-$ peak ($\sim$1570 cm^{-1}), along with a D band ($\sim$1350 cm^{-1}). We show that the typical Raman signals for SWNTs are the signature of their helical structure determined using density functional theory simulation and structural analysis for hydrogenated and dehydrogenated SWNT samples. We demonstrate that the G$^-$ mode at $\sim$1570 cm^{-1} is unique to opened tubular graphene structures of $\sim$2 nm diameter. We also demonstrate that the D mode of $\sim$1350 cm^{-1} is originated from edge defects of opened SWNTs, revealing strong eigenvectors, which is absent in concentric tubes. We also report a radial−tangential mode (RTM) for concentric and opened SWNTs, which appears following RBM. We also interpret the low-energy Raman signal, reported as an RBM band, to be convolution of "localized RBM" ($\sim$170 cm^{-1}) and RTM ($\sim$190 cm^{-1}) for helical SWNTs. We also show that the analysis of the Raman spectra of SWNTs is consistent with general understanding on Raman analysis of carbon materials.
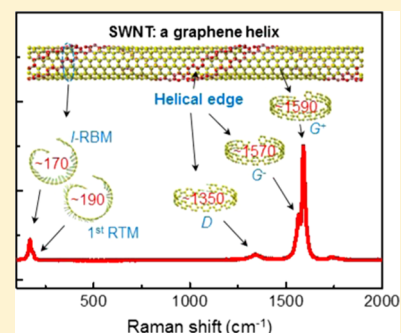
INTRODUCTION

Raman spectroscopy provides ultimate information to manifest structures of matter[1−3] because phonon behaviors of the atoms are sensitive to atomic-level changes. Radial breathing mode (RBM) of single-walled carbon nanotubes (SWNTs) has been understood to be originated from synchronous radial vibration of carbon atoms (i.e., contraction and expansion) in perpendicular to the tube's axis.[1,2,4,5] It is a general understanding that each peak comprising the RBM band indicates diameters of SWNTs.[1−14] The availability of the RBM band to measure diameters has been extended to evaluate the electronic properties, i.e., metallic or semiconducting, with the chiral theory of carbon nanotubes (CNTs),[15] where the diameters of CNTs are correlated with chirality. However, the low-energy Raman signals have been reported from graphene structures[16−18] as well as thin nanographite comprising a few layers of graphene.[19] Lee et al. have shown that low-energy Raman signals of graphene structures (interpreted as RBM) are due to the radial mode (RM) formed by end curvatures of graphene of $\sim$2.2 nm diameter.[20] The RM model, where eigenvectors head for the center of the curvature of graphene structures, covers the RBM hypothesis of SWNTs. This indicates that the low-energy

Raman signals are not unique to SWNTs and thus cannot be evidence for the tubular graphene structures.

The appearance of a D band, which is associated with defects of crystalline sp^2 carbon structures,[21,22] has not been clearly addressed for SWNTs. Sophisticated Raman study on the D mode in graphene structures shows that it does not appear at the center of graphene, but from the edges.[21] The results suggest that the D mode is originated from the edge defects of graphene, which is consistent with the general understanding on Raman analysis for graphite.[22] Well-crystallized SWNTs should not reveal the D band because the edge area is negligible due to their atomic thickness and higher aspect ratio ($>$1000), if the one-dimensional matter is a concentric tube. The origin of a G$^-$ peak, which is indeed unique to SWNTs, is also not established yet,[1−9] although the signal has been understood to be related to the curvature (i.e., diameter) of tube and thus contains information about electronic properties of SWNTs with respect to chiral theory like RBM. The G$^-$ peak typically appears at $\sim$1570 cm^{-1} as red shift and is unseparated from the G$^+$ peak at $\sim$1590 cm^{-1}, although it is diverse in shape.[23] With the scientific

uncertainties for D and G⁻ signals, there is substantial contradiction on SWNTs. Diameters of SWNTs (0.5–1.5 nm for 120–370 cm⁻¹) measured from the low-energy Raman signals[1,3–9] are too small compared to those (1.4–2.5 nm) directly observed by a high-resolution transmission electron microscope (HRTEM).[24–28]

Lee et al. reported that SWNTs adopting a graphene helix resulted from spiral growth of a zigzag graphene nanoribbon (Figure S1, Supporting Information).[27] The prevailing nodal morphology in HRTEM[24–30] and scanning tunneling microscopy[31,32] images provides morphological evidence for the helical structure model of SWNTs (Figures S1–S3, Supporting Information). In this paper, we reveal Raman spectra for SWNTs with simulations for concentric and opened SWNT structures and a complementary analysis including HRTEM observation, IR spectroscopy, and measurement for hydrogenated samples. The typical RBM and D bands as well as the G⁻ peak are evidence for the helical structure of SWNTs.

■ EXPERIMENTAL SECTION

We studied commercial (arc-discharge) SWNTs (Hanwha Chemical, South Korea) (Figure S4, Supporting Information). Purified and unpurified SWNT samples were used for the hydrogenation experiment and HRTEM observation, respectively. Purified SWNTs appear as bundles, whereas unpurified samples reveal some SWNTs existing individually. For HRTEM observation, unpurified SWNTs were sonicated under a high ultrasonic power density of 20 W/mL for 2 h. The samples were observed with two HRTEM apparatus: (i) an aberration-corrected energy-filtered TEM (200 kV, Libra200 HT Mc Cs TEM; Carl Zeiss) and (ii) a conventional HRTEM (JEOL JEM-2100F). The latter was used for the electron beam irradiation experiment. For the electron beam irradiation experiment during HRTEM observation, the current density was kept between 49 and 137 pA/cm². Irradiation (49 pA/cm²) was applied to the isolated tubules (where a side is free) to minimize the vibration of the samples. Dehydrogenation for purified SWNTs was performed in a vacuum furnace, kept at 600 °C under high vacuum (10⁻⁵ Torr) for 30 min. The dehydrogenated SWNTs, prepared on a molybdenum substrate, were exposed to the direct current (DC) H-plasma in a chemical vapor deposition chamber for 10 min for hydrogenation. Gas pressure was kept at 50 Torr where a high-density DC plasma (gas temperature is ∼3000 °C) is generated.[33] The substrate was kept at a temperature of 600 °C, and a H₂ gas flow of 200 sccm was maintained. To confirm reversibility, we performed a cycle of hydrogenation and dehydrogenation showing the absence and reappearance of the RM band. We also analyzed SWNTs before and after hydrogenation with IR (Thermo Scientific NICOLET iS10) and Raman (Renishaw inVia Raman microscope) techniques. The excitation energy of the Raman laser was 532 nm (a spot size of 1–2 μm), and its power density was 1.6 mW/μm². The Raman RM peak was deconvoluted by the Origin program (OriginPro 8.6).

We carried out simulations from an armchair (15,15) SWNT (∼2.0 nm in diameter) and opened tube structures modified from armchair SWNTs using density functional theory (DFT) as implemented in the Quantum ESPRESSO simulation package.[34] Comparative electronic structure calculations were carried out on a helical structure, modified from the armchair (6,6) tube (∼0.82 nm), with and without hydrogenation. Generalized gradient approximation was used

for exchange−correlation energy of electrons and ultrasoft pseudopotentials to represent the interaction between ionic cores and valence electrons.[35,36] Kohn−Sham wave functions were represented with a plane wave basis with an energy cutoff of 40 Ry and charge density cutoff of 240 Ry.[37] Integration over a Brillouin zone (BZ) was sampled with a mesh of $1 \times 1 \times 2$ grid.[38] Dynamical matrices at the Γ point ($q = 0$) in BZ were computed by a perturbative linear response approach used in DFT.

■ RESULTS AND DISCUSSION

Helical SWNT reveals traces of a graphene helix, i.e., locally discontinuous wall lattices,[24,25] as depicted in Figure 1. The
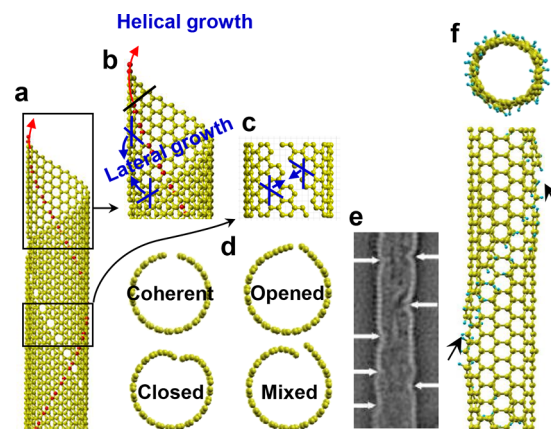
Figure 1. Schematic explaining helical structures of a SWNT. (a−c) Schematic explaining helical and lateral growth of a SWNT. Blue lines indicate closest-packed zigzag lines driving the helical and lateral growth. (d, e) Schematic showing four typical cross sections (coherent, opened, closed, and mixed) for helical SWNT (d), which are modeled from Meyer et al.'s HRTEM image (reproduced with permission from The Royal Microscopical Society, ref 25) (e) where helical features (arrows) are evident. (f) Simulated structure model of a hydrogenated helical SWNT. Carbon and hydrogen atoms are shown in yellow and blue, respectively. Arrows in (f) indicate the disconnected sections.

helical traces of the SWNT samples are evident in HRTEM observation (Figure S4, Supporting Information). The helical features are also evident when the samples are irradiated by electron beam using a conventional HRTEM (working at 200 kV) (Figure S5, Supporting Information). The traces of graphene helices become more prominent when cross-linked SWNTs are exposed to electron beam (137 pA/cm²) for 6 min. The experiment explains electron beam bending of coherently scrolled SWNTs[28] as well as mobile defects during in situ HRTEM observation with electron beam irradiation for SWNTs (Figure S6, Supporting Information)[39] (dual helical traces revealed from both bottom and top graphene walls can be seen as mobile defects). The diameters of the tubules are measured to be ∼1.8 nm in this study, which are in the range of diameters of SWNTs, 1.5−2.5 nm, reported by HRTEM observation in the literature.[24–28]

Figure 2 shows Raman spectra obtained from SWNT samples analyzed in this study. The dehydrogenated sample reveals a clear low-energy band between ∼120 and ∼200 cm⁻¹ (comprising a strong peak at 168 cm⁻¹ and a shoulder peak at 186 cm⁻¹), a D band at ∼1350 cm⁻¹, and a strong G band at 1530−1630 cm⁻¹. The low-energy band is also observable
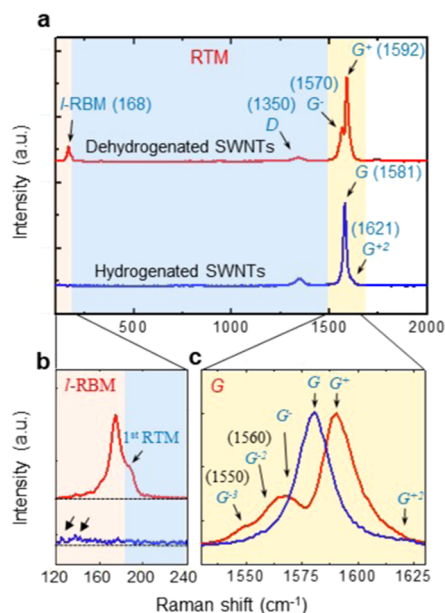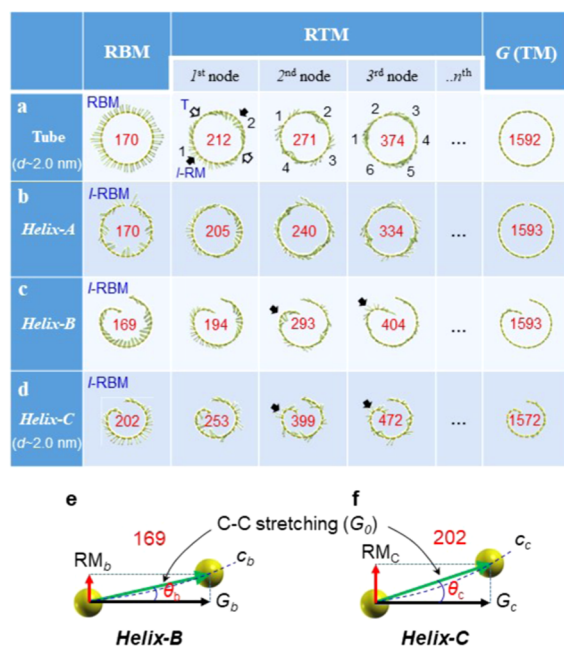
Figure 2. Raman spectra for hydrogenated and dehydrogenated SWNT samples. (a) Raman spectra where D and G bands are evident. Radial−tangential mode (RTM) is placed between RBM (localized RBM, l-RBM) and G. The dotted line indicates the position of G for graphite (i.e., 1581 cm^{-1}). (b, c) Expanded Raman spectra in the low-energy range and in the range of 1530−1630 cm^{-1}, where G^{-3}, G^{-}, and G^{+2} peaks are interpreted to be unique to helical SWNTs.

Figure 3. Simulated Raman-active modes for concentric and opened SWNTs and vector diagrams. (a−d) RBM, RTMs, and G for a concentric SWNT (a) and opened SWNTs (b−d). Diameter of the concentric tube, helix-A, and helix-B is ∼2 nm, whereas that of helix-C is ∼1.4 nm. Black numbers indicate the number of l-RMs. "T" indicates tangential eigenvectors. Each RTM is composed of radial and tangential eigenvectors and is featured by l-RMs. (e, f) Vector diagrams elucidating the relationship between G and RBM (l-RBM) with respect to the angle (θ) formed by two dislocated atoms (see Table 1). The diameter and curvature of the graphene structures are indicated by d and c ($1/d$), respectively. Red numbers indicate frequencies for each mode.

from Raman spectra of purified and pre-dehydrogenated samples. The G^{-} peak[1−12] unique to SWNTs is evident at 1570 cm^{-1}, split from the strongest G^{+} peak at 1590 cm^{-1}. With hydrogenation, the low-energy band disappears but other signals remain unaltered, except for shift of the G^{+} peak to 1581 cm^{-1} (G) (Figure S7, Supporting Information). Only the dehydrogenated sample reveals the unique G^{-} peak at 1570 cm^{-1}, whereas the other samples reveal a weak signal near 1621 cm^{-1} (Figure 2b), assigned to G^{+2}. Strong sp^3 C−H stretching signals at about 2850, 2920, and 2955 cm^{-1} are evident in the IR spectrum of hydrogenated SWNTs[40−42] (Figure S8, Supporting Information). The IR sp^3 C−H stretching signals disappear with dehydrogenation.

Raman-active modes for concentric and opened SWNTs are shown in Figure 3. Concentric SWNT of a diameter of 2 nm reveals RBM at 170 cm^{-1}, which is the perfect resonant condition dominated by pure radial eigenvectors. For opened SWNTs, localized RBM (l-RBM), where a part of the eigenvectors is decentered (Figure 3b−d), is evident. Both structures reveal a unique "radial−tangential mode (RTM)", which is the combination of radial and tangential eigenvectors (Figure 3a−d). RTM appears in order following RBM (l-RBM) (Figure S9, Supporting Information) and reveals localized RMs (l-RMs) of 2n, where n is the number of nodes. Each RTM is dominated by "localized RM (l-RM)" (solid arrows in Figure 3), where a set of eigenvectors head for decentered points similar to that of l-RBM. Clear l-RMs are evident at the high mode of ∼400 cm^{-1} from the steep-end curvatures in helix-B and helix-C (solid arrows in Figure 3c,d series), although l-RM becomes gradually weaker with the increase of mode.

The dramatic variation of Raman signals with hydrogenation and dehydrogenation[40−42] (unanswered with the conventional concentric tubular structure) can be explained by the helical

structure model (Figure S1, Supporting Information). With the simulation data (Figure 3) and the value of RM calculated from the vector diagram (Table 1), we assign the strong low-

Table 1. Calculated l-RBM and G Frequencies^a

diameter	θ (deg.)	l-RBM (cm^{-1})	G (cm^{-1})
2.0 nm (helix-B)	∼6	∼166	∼1581
1.4 nm (helix-C)	∼7	∼194	∼1578

^{a}The data show that the curvature of tubular graphene (related with θ) can be estimated from Raman G and l-RBM signals, similar to the case of RBM hypothesis based on the concentric tube structure. l-RBM = G$_0 \sin \theta$ and G = G$_0 \cos \theta$, where G$_0$ is 1590 cm^{-1} for G^{+} measured.

energy peak at ∼168 cm^{-1} and the shoulder peak at ∼186 cm^{-1} of the dehydrogenated sample to l-RBM and 1st RTM of a helical SWNT, respectively. We attribute the disappearance of the low-energy band from hydrogenated samples to van der Waals zipping of the graphene helix via sp^3 C−H bonds formed on the both helical edges (Figure 1f) during hydrogenation. Due to helical and subsequent lateral growth, a SWNT produces diverse local edges (Figure 1d) of which the unrolled width becomes the diameter (Figure S1, Supporting Information). With the physical zipping, the edges of a dehydrogenated graphene helix unify and rearrange (like coalescence of bubbles with a smallest agitation), producing a bumpy and asymmetric structure that may lack the l-RBM and RTM resonance conditions. This explains the weak signals
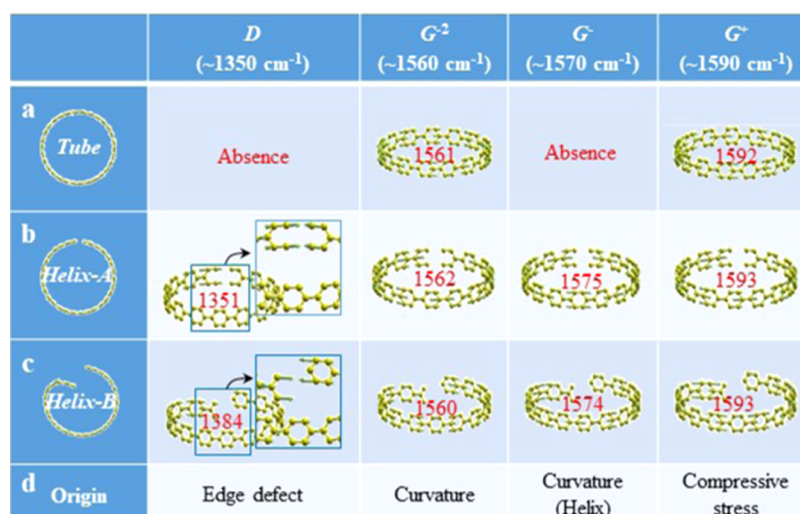
Figure 4. Simulated Raman-active D, G^{-2}, G^-, and G^+ modes for concentric and opened SWNTs. (a–c) Modes for concentric (a) and opened (b, c) SWNTs. Insets in (b, c) reveal strong eigenvectors evolved from edges of D modes. Red numbers indicate frequencies for each mode. (d) Origin of each mode.

Table 2. Measured and Simulated Raman Frequencies of l-RBM (RBM), RTM (1st RTM), D, and G Bands for Different SWNT Structures[a]

	l-RBM	1st RTM	D	G^{-3}	G^{-2}	G^-	G	G^+	G^{+2}
					unit: cm^{-1}				
measured	168	186	~1350	~1550	~1560	~1570	~1581	~1590	~1621
helix-A	163	193	1351	1550	1562	1575		1593	1621
helix-B	169	194	1384	1549	1560	1574		1593	1620
tube	170	212			1561			1592	
graphite[b]			1350				1580		

[a]The data for the opened tube structure are identical to those measured from SWNT samples but are clearly different from those for the concentric tube structure. [b]Data for graphite were quoted from ref 13.

between 100 and ~170 cm^{-1} in the Raman spectrum of the hydrogenated sample (arrows in Figure 2b). Further simulation also shows enlargement in the diameter of an even coherently scrolled helical structure by ~10% with hydrogenation (Figure S10, Supporting Information), supporting the red shift of the RM signals. Dehydrogenation can make graphene helices release (unzipping) from pinning up by sp³ C−H bonds and recover original curvatures, explaining the reappearance of the low-energy band (Figure S7, Supporting Information) as well as the G⁻ peak that splits from G⁺.

Strong eigenvectors at both edges of graphene are evident from the D modes shown in Figure 4b,c. The data indicate the origin of the D band for SWNTs to be edges of graphene, and this is consistent with the general formation mechanism for the D band that has been established from graphene or graphite.[21,22] The natural instability of the edge of atomic-thick graphene helices may not reveal a unique Raman signal, explaining the broad band ranging 1300−1400 cm^{-1} for SWNTs. On the other hand, simulation data for G modes demonstrate that the G⁻ peak at ~1570 cm^{-1} (G⁺ at ~1590 cm^{-1}) is a signature of the helical structure of SWNTs because it is absent for the tubular structure (Figure 4 and Table 2). All G peaks between 1530 and 1630 cm^{-1} are ~1550, ~1560, ~1570, ~1581, ~1590, ~1600, ~1610, and ~1621 cm^{-1}, which are assigned to G⁻³, G⁻², G⁻, G, G⁺, and G⁺² modes, respectively, where ~1550 (G⁻³), ~1570 (G⁻), and ~1621 cm^{-1} (G⁺²) peaks are unique to the helical structure. The results elucidate the unanswered origin of G⁻ signals to be the

uneven helical curvature (see Figure 1). With the data of D, this analysis provides strong evidence for the helical structure of SWNTs.

The red shift of G modes is supported by the conventional mechanism for the Raman shift with stress[43] in condensed matter where the presence of dislocation and vacancy causes tensile stress, letting peaks shift to the left. The helical graphene structure can be considered as a graphene tube with a helical dislocation; thus, the atoms in an edge zone can be under tensile stress. The appearance of a unified G peak at 1581 cm^{-1} for hydrogenated SWNTs (which is between 1570 and 1590 cm^{-1}) corresponds to that of unstressed graphene or graphite.[3,21,22] The data indicate that the hydrogenated and enlarged helical structure is free from compressive stress, which may be applied to the samples during dehydrogenation. With simulation data, we assign the peak at ~1560 cm^{-1} to the G⁻² peak, which generally appears from SWNTs.[1,2,5,9,14] Appearance of the red-shifted G peaks (including the G⁻² peak) can also be explained by the vector diagram (Figure 3e,f).

Some reports explained that sp³ C−H bonds can be formed on the wall of SWNTs.[42] However, this may be impossible because the potential energy for the formation of sp³ C−H bonds on the surface of graphene is very high, up to 1.0−3.3 eV.[44] With the helical structure of SWNTs, it is reasonable that the sp³ C−H bonds are formed at the edges of graphene helices (Figure 1f). The edges provide ideal sites for sp² and sp³ chemical bonds because the bonding can decrease the surface energy of the SWNTs. The atoms on the hydrogenated

edges are constrained,[45] which explains the evolution of a weak G^{+2} peak at ~1621 cm^{-1} (Figure 2a,c). The peak is also evident from purified and pre-dehydrogenated samples (Figure S7, Supporting Information). This is reasonable because C−H bonds are formed during synthesis of SWNTs and thus exist in the samples unless the dehydrogenation treatment is carried out.

Our Raman analysis based on the helical structure explains the diverse low-energy Raman signals for SWNTs in the literature. Edges of the graphene helix are naturally unstable, and thus, SWNTs are prone to energy (as confirmed by the electron beam irradiation experiment), and Raman signals can be affected by the synthesis technique, laser excitation lines,[4,9,11−13] laser power,[46] and environmental factors[46] such as bundled or isolated (suspended[47,48] or deposited[16,49] on a substrate). For example, the enlargement of HiPco SWNTs estimated from the low-energy signals after 1800 °C heat treatment reported by Yudasaka et al.[50] can be explained with our helical structure model. After stepwise heating up to 1800 °C, the edge structure of helical SWNTs may rearrange, resulting in regular changes in Raman signals. Practically, enlargement of concentric tubes after heat treatment is nonphysical, and this is left unanswered. Also, the simulation data for highly deformed helical structures (helix-B and helix-C in Figure 3) reveal striking l-RM eigenvectors even at higher frequencies up to 472 cm^{-1} due to localized steep curvatures of the edge of a graphene helix. Indeed, our model explains the underestimated diameters of SWNTs (0.5−1.5 nm),[1−15] measured from the low-energy Raman signals, i.e., l-RBM and l-RM, suggesting that our helical geometry may be a universal structure of SWNTs. Also, the appearance of the G peak at 1581 cm^{-1} for hydrogenated SWNTs, which is identical to that of graphene materials (1580−1582 cm^{-1})[3,17,18,43] meaning free from stress, provides general evidence for our Raman analysis of SWNTs based on the helical structure. The diverse structures reported[24−32,39] provide natural evidence for our helix model for SWNTs, where each sample as well as every part of the sample is different in structure.

Simulation of the electronic density of states (DOS) shows that a zigzag graphene helix is metallic in nature and becomes a semiconductor with a finite band gap of ~1.45 eV with hydrogenation (Figure 5). The dangling bond at the edge carbon atom gets passivated with a hydrogen atom and shares the electrons. Thus, the 2p orbitals of carbon atoms get pushed away from the Fermi level, opening a gap. Also, we expect that distortion of metallic graphene may produce band gap[51] due to the helical and lateral growth. These explain diverse electronic
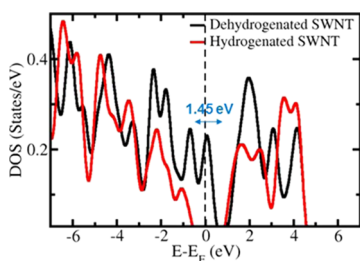
properties including semiconducting with different band gaps in the literature.[32]

In summary, the typical Raman signals of SWNTs are of helical graphene, where the appearance of the G$^-$ peak and D band becomes its evidence. Our l-RBM and RTM models explain the diverse low-energy Raman signals as well as the underestimated diameters of SWNTs for the last 20 years (0.5−1.3 nm calculated from RBM signals compared to 1.4−2.5 nm measured from HRTEM observation). The results provide a way of engineering one-dimensional materials and understanding the nature of other graphene materials via Raman analysis.

■ ASSOCIATED CONTENT

ⓢ Supporting Information

The Supporting Information is available free of charge on the ACS Publications website at DOI: 10.1021/acs.jpcc.9b02174.

Structural analysis for SWNTs and detailed Raman simulation data for concentric and opened tubular graphene structures; helical growth model of SWNTS; previously reported HRTEM and STM images of SWNTs; HRTEM observation of SWNTs; Raman spectra for purified, pre-dehydrogenated, hydrogenated, and dehydrogenated SWNTs; IR spectra of purified, hydrogenated, and dehydrogenated SWNTs; and simulated Raman-active modes for concentric and opened SWNTs (PDF)

■ AUTHOR INFORMATION

Corresponding Author

*E-mail: jklee@kist.re.kr.

ORCID ⓘ

Wooyoung Lee: 0000-0001-8406-4324

Present Address

▽Opto-Electronic Materials and Devices Research Center, Korea Institute of Science and Technology, Seoul 02792, Republic of Korea (Y.P.).

Author Contributions

#Y.P. and K.P.S.S.H. contributed equally to this work.

Notes

The authors declare no competing financial interest.

■ ACKNOWLEDGMENTS

Figure 5. Simulated electronic DOS for a helical SWNT. With hydrogenation, the metallic helical structure becomes a semiconductor with a band gap of 1.45 eV. Simulations were performed from the model shown in Figure 1f.

■ REFERENCES

(1) Dresselhaus, M. S.; Dresselhaus, G.; Saito, R.; Jorio, A. Raman spectroscopy of carbon nanotubes. *Phys. Rep.* **2005**, *409*, 47−99.

(2) Jorio, A.; Pimenta, M. A.; Filho, A. G. S.; Saito, R.; Dresselhaus, G.; Dresselhaus, M. S. Characterizing carbon nanotube samples with resonance Raman scattering. *New J. Phys.* **2003**, *5*, No. 139.

(3) Hodkiewicz, J. et al. *Characterizing graphene with Raman spectroscopy*; Thermo Fisher Scientific: Madison, WI, 2010.

(4) Maultzsch, J.; Telg, H.; Reich, S.; Thomsen, C. Radial breathing mode of single-walled carbon nanotubes: Optical transition energies and chiral-index assignment. *Phys. Rev. B* **2005**, *72*, No. 205438.

(5) Rao, A. M.; Richter, E.; Bandow, S.; Chase, B.; Eklund, P. C.; Williams, K. A.; Fang, S.; Subbaswamy, K. R.; Menon, M.; Thess, A.;

et al. Diameter-selective Raman scattering from vibrational modes in carbon nanotubes. *Science* **1997**, *275*, 187−191.

(6) Kataura, H.; Kumazawa, Y.; Maniwa, Y.; Ohtsuka, Y.; Sen, R.; Suzuki, S.; Achiba, Y. Diameter control of single-walled carbon nanotubes. *Carbon* **2000**, *38*, 1691−1697.

(7) Ando, Y.; Zhao, X.; Hirahara, K.; Suenaga, K.; Bandow, S.; Iijima, S. Arc plasma jet method producing single-wall carbon nanotubes. *Diamond Relat. Mater.* **2001**, *10*, 1185−1189.

(8) Kajiura, H.; Tsutsui, S.; Huang, H.; Murakami, Y. High-quality single-walled carbon nanotubes from arc-produced soot. *Chem. Phys. Lett.* **2002**, *364*, 586−592.

(9) Kataura, H.; Kumazawa, Y.; Maniwa, Y.; Umezu, I.; Suzuki, S.; Ohtsuka, Y.; Achiba, Y. Optical properties of single-wall carbon nanotubes. *Synth. Metals* **1999**, *103*, 2555−2558.

(10) Rodriguez, R. D.; Blaudeck, T.; Kalbacova, J.; Sheremet, E.; Schulze, S.; Adner, D.; Hermann, S.; Hietschold, M.; Lang, H.; Schulz, S. E.; et al. Metal nanoparticles reveal the organization of single-walled carbon nanotubes in bundles. *RSC Adv.* **2016**, *6*, 15753−15758.

(11) Chen, G.; Sumanasekera, G. U.; Pradhan, B. K.; Gupta, R.; Eklund, P. C.; Bronikowski, M. J.; Smalley, R. E. Raman-Active Modes of Single-Walled Carbon Nanotubes Derived from the Gas-Phase Decomposition of CO (HiPco Process). *J. Nanosci. Nanotechnol.* **2002**, *2*, 621−626.

(12) Bachilo, S. M.; Strano, M. S.; Kittrell, C.; Hauge, R. H.; Smalley, R. E.; Weisman, R. B. Structure-assigned optical spectra of single-walled carbon nanotubes. *Science* **2002**, *298*, 2361−2366.

(13) Kuzmany, H.; Plank, W.; Hulman, M.; Kramberger, Ch.; Gruneis, A.; Pichler, Th.; Peterlik, H.; Kataura, H.; Achiba, Y. Determination of SWCNT diameters from the Raman response of the radial breathing mode. *Eur. Phys. J. B* **2001**, *22*, 307−320.

(14) Hennrich, F.; Krupke, R.; Lebedkin, S.; Arnold, K.; Fischer, R.; Resasco, D. E.; Kappes, M. M. Raman spectroscopy of individual single-walled carbon nanotubes from various sources. *J. Phys. Chem. B* **2005**, *109*, 10567−10573.

(15) Dresselhaus, M. S.; Dresselhaus, G.; Saito, R. Physics of carbon nanotubes. *Carbon* **1995**, *33*, 883−891.

(16) Podila, R.; Rao, R.; Tsuchikawa, R.; Ishigami, M.; Rao, A. M. Raman spectroscopy of folded and scrolled graphene. *ACS Nano* **2012**, *6*, 5784−5790.

(17) He, R.; Chung, T. F.; Delaney, C.; Keiser, C.; Jauregui, L. A.; Shand, P. M.; Chancey, C. C.; Wang, Y.; Bao, J.; Chen, Y. P. Observation of low energy Raman modes in twisted bilayer graphene. *Nano Lett.* **2013**, *13*, 3594−3601.

(18) Verzhbitskiy, I. A.; Corato, M. D.; Ruini, A.; Molinari, E.; Narita, A.; Hu, Y.; Schwab, M. G.; Bruna, M.; Yoon, D.; Milana, S.; et al. Raman fingerprints of atomically precise graphene nanoribbons. *Nano Lett.* **2016**, *16*, 3442−3447.

(19) Wang, J. J.; Zhu, M. Y.; Outlaw, R. A.; Zhao, X.; Manos, D. M.; Holloway, B. C.; Mammana, V. P. Free-standing subnanometer graphite sheets. *Appl. Phys. Lett.* **2004**, *85*, 1265−1267.

(20) Lee, J.-K.; Hembram, K. P. S. S.; Park, Y.; Lee, S.-G.; Kim, J.-G.; Lee, W.; Moon, D. J. Raman Radial Mode Revealed from Curved Graphene. *J. Phys. Chem. Lett.* **2017**, *8*, 2597−2601.

(21) Ferrari, A. C.; Meyer, J. C.; Scardaci, V.; Casiraghi, C.; Lazzeri, M.; Mauri, F.; Piscanec, S.; Jiang, D.; Novoselov, K. S.; Roth, S.; et al. Raman Spectrum of Graphene and Graphene Layers. *Phys. Rev. Lett.* **2006**, *97*, No. 187401.

(22) Pimenta, M. A.; Dresselhaus, G.; Dresselhaus, M. S.; Cançado, L. G.; Jorio, A.; Saito, R. Studying disorder in graphite-based systems by Raman spectroscopy. *Phys. Chem. Chem. Phys.* **2007**, *9*, 1276−1290.

(23) Jorio, A.; Filho, A. G. S.; Dresselhaus, G.; Dresselhaus, M. S.; Swan, A. K.; Ünlü, M. S.; Goldberg, B. B.; Pimenta, M. A.; Hafner, J. H.; Lieber, C. M.; et al. G-band resonant Raman study of 62 isolated single-wall carbon nanotubes. *Phys. Rev. B* **2002**, *65*, No. 155412.

(24) Suenaga, K.; Sato, Y.; Liu, Z.; Koshino, M.; Jin, C. HR-TEM of Carbon Network, Towards Individual CC Bond Imaging. *JEOL News* **2009**, *44*, 32−37.

(25) Meyer, R. R.; Friedrichs, S.; Kirkland, A. I.; Sloan, J.; Hutchison, J. L.; Green, M. L. H. A composite method for the determination of the chirality of single walled carbon nanotubes. *J. Microsc.* **2003**, *212*, 152−157.

(26) Hashimoto, A.; Suenaga, K.; Gloter, A.; Urita, K.; Iijima, S. Direct evidence for atomic defects in graphene layers. *Nature* **2004**, *430*, 870−873.

(27) Lee, J.-K.; Lee, S.; Kim, J.-G.; Min, B.-K.; Kim, Y.-I.; Lee, K.-I.; An, K. H.; John, P. Structure of single-wall carbon nanotubes: A graphene helix. *Small* **2014**, *10*, 3283−3290.

(28) Warner, J. H.; Young, N. P.; Kirkland, A. I.; Briggs, G. A. D. Resolving strain in carbon nanotubes at the atomic level. *Nat. Mater.* **2011**, *10*, 958−962.

(29) Thess, A.; Lee, R.; Nikolaev, P.; Dai, H.; Petit, P.; Robert, J.; Xu, C.; Lee, Y. H.; Kim, S. G.; Rinzler, A. G.; et al. Crystalline Ropes of Metallic Carbon Nanotubes. *Science* **1996**, *273*, 483−487.

(30) Journet, C.; Maser, W. K.; Bernier, P.; Loiseau, A.; Chapelle, M. L.; Lefrant, S.; Deniard, P.; Lee, R.; Fischer, J. E. Large-scale production of single-walled carbon nanotubes by the electric-arc technique. *Nature* **1997**, *388*, 756−758.

(31) Ge, M.; Sattler, K. Scanning tunneling microscopy of single-shell nanotubes of carbon. *Appl. Phys. Lett.* **1994**, *65*, 2284−2286.

(32) Wilder, J. W. G.; Venema, L. C.; Rinzler, A. G.; Smalley, R. E.; Dekker, C. Electronic structure of atomically resolved carbon nanotubes. *Nature* **1998**, *391*, 59−62.

(33) Lee, J.-K.; Lee, S.; Kim, Y.-I.; Kim, J.-G.; Min, B.-K.; Lee, K.-I.; Park, Y.; John, P. The seeded growth of graphene. *Sci. Rep.* **2014**, *4*, No. 5682.

(34) Giannozzi, P.; Baroni, S.; Bonini, N.; Calandra, M.; Car, R.; Cavazzoni, C.; Ceresoli, D.; Chiarotti, G. L.; Cococcioni, M.; Dabo, I.; et al. QUANTUM ESPRESSO: A modular and open-source software project for quantum simulations of materials. *J. Phys.: Condens. Matter* **2009**, *21*, No. 395502.

(35) Perdew, J. P.; Burke, K.; Ernzerhof, M. Generalized gradient approximation made simple. *Phys. Rev. Lett.* **1996**, *77*, 3865−3868.

(36) Vanderbilt, D. Soft self-consistent pseudopotentials in a generalized eigenvalue formalism. *Phys. Rev. B* **1990**, *41*, 7892−7895.

(37) Monkhorst, H. J.; Pack, J. D. Special points for Brillouin-zone integrations. *Phys. Rev. B* **1976**, *13*, 5188−5192.

(38) Methfessel, M.; Paxton, A. High-precision sampling for Brillouin-zone integration in metals. *Phys. Rev. B* **1989**, *40*, 3616−3621.

(39) Warner, J. H.; Schäffel, F.; Zhong, G.; Rümmeli, M. H.; Büchner, B.; Robertson, J.; Briggs, G. A. D. Investigating the Diameter-Dependent Stability of Single-Walled Carbon Nanotubes. *ACS Nano* **2009**, *3*, 1557−1563.

(40) Zhang, G.; Qi, P.; Wang, X.; Lu, Y.; Mann, D.; Li, X.; Dai, H. Hydrogenation and hydrocarbonation and etching of single-walled carbon nanotubes. *J. Am. Chem. Soc.* **2006**, *128*, 6026−6027.

(41) Nikitin, A.; Ogasawara, H.; Mann, D.; Denecke, R.; Zhang, Z.; Dai, H.; Cho, K.; Nilsson, A. Hydrogenation of single-walled carbon nanotubes. *Phys. Rev. Lett.* **2005**, *95*, No. 225507.

(42) Meletov, K. P.; Maksimov, A. A.; Tartakovskii, I. I.; Bashkin, I. O.; Shestakov, V. V.; Krestinin, A. V.; Shulga, Y. M.; Andrikopoulos, K. S.; Arvanitidis, J.; Christofilos, D.; et al. Raman study of the high-pressure hydrogenated single-wall carbon nanotubes: In search of chemically bonded and adsorbed molecular hydrogen. *Chem. Phys. Lett.* **2007**, *433*, 335−339.

(43) Mohiuddin, T. M. G.; Lombardo, A.; Nair, R. R.; Bonetti, A.; Savini, G.; Jalil, R.; Bonini, N.; Basko, D. M.; Galiotis, C.; Marzari, N.; et al. Uniaxial strain in graphene by Raman spectroscopy: G peak splitting, Grüneisen parameters, and sample orientation. *Phys. Rev. B* **2009**, *79*, No. 205433.

(44) Miura, Y.; Kasai, H.; Diño, W.; Nakanish, H.; Sugimoto, T. First principles studies for the dissociative adsorption of H_2 on graphene. *J. Appl. Phys.* **2003**, *93*, 3395−3400.

(45) Choe, D. H.; Bang, J.; Chang, K. J. Electronic structure and transport properties of hydrogenated graphene and graphene nanoribbons. *New J. Phys.* **2010**, *12*, No. 125005.

(46) Fantini, C.; Jorio, A.; Souza, M.; Strano, M. S.; Dresselhaus, M. S.; Pimenta, M. A. Optical transition energies for carbon nanotubes from resonant Raman spectroscopy: Environment and temperature effects. *Phys. Rev. Lett.* **2004**, *93*, No. 147406.

(47) Zhang, Y.; Zhang, J.; Son, H.; Kong, J.; Liu, Z. Substrate-induced Raman frequency variation for single-walled carbon nanotubes. *J. Am. Chem. Soc.* **2005**, *127*, 17156−17157.

(48) Meyer, J. C.; Paillet, M.; Michel, T.; Moréac, A.; Neumann, A.; Duesberg, G. S.; Roth, S.; Sauvajol, J.-L. Raman modes of index-identified freestanding single-walled carbon nanotubes. *Phys. Rev. Lett.* **2005**, *95*, No. 217401.

(49) Dresselhaus, M. S.; Dresselhaus, G.; Jorio, A.; Filho, A. G. S.; Saito, R. Raman spectroscopy on isolated single wall carbon nanotubes. *Carbon* **2002**, *40*, 2043−2061.

(50) Yudasaka, M.; Kataura, H.; Ichihashi, T.; Qin, L.-C.; Kar, S.; Iijima, S. Diameter enlargement of HiPco single-wall carbon nanotubes by heat treatment. *Nano Lett.* **2001**, *1*, 487−489.

(51) Bu, W.; Jiang, J.; Dong, J. Localization length in deformed metallic carbon nanotubes. *Phys. Lett. A* **2002**, *302*, 125−130.